J Mater Sci (2011) 46:7806–7814
DOI 10.1007/s10853-011-5761-8

Influence of oxides on the stability of zinc foam

Avinash Chethan · Francisco Garcia-Moreno · Nelia Wanderka · B. S. Murty · John Banhart

Received: 21 March 2011 / Accepted: 30 June 2011 / Published online: 14 July 2011

Abstract The influence of oxides on the stabilisation of zinc foam made by foaming-compacted powder mixtures has been investigated by varying the oxide content in the zinc powder used by oxidation and reduction. Optical, scanning electron and transmission electron microscopy as well as energy dispersive X-ray mapping were used to determine the oxide distribution, morphology and structure in the foams. The study revealed that with increase in the oxide content of the foam, the maximum expansion and expansion rate increased. Small amount of nano-sized oxide particles and their cluster, which are randomly distributed, were observed within the bulk of foam. But the major fraction of oxides is observed on the surface of pores in the form of clusters. These clusters are distributed uniformly all over the surface. Effect of these oxides on the stability of foam is discussed. The formation of satellite pores, which is characteristic signature of zinc foams, and their stability, is investigated.

Introduction

Metal foams have emerged as a popular field of research owing to the technological relevance of such lightweight materials, which exhibit an unprecedented spectrum of properties and also due to the interesting physics that govern the foaming process of metals. Given their special structure and low weight, they have enormous potential for many applications in various industrial sectors [1–3].

Metal foams are produced mainly by two processes: melt route and powder (metallurgical) route. In the former, gas is bubbled through a highly viscous liquid alloy, leading to the formation of foams, whereas in the latter, metal powder/blowing agent mixtures are first compacted and then foamed by heating to high temperature. One of the key factors in both cases is the stabilisation of the evolving foam structure, which ensures that the energetically unfavourable arrangement of a high internal surface area survives [4]. For the melt route, the action of particles immersed in the melt is widely accepted as main stabilisation mechanism [5–7]. In the powder route, oxides are found to be a prerequisite for stabilisation, but their exact action is not sufficiently well known [8–11].

The kinetic stability of powder route foams has been under investigation for some time. Weber observed oxide particles in regions close to the surface of solid cell walls and postulated that accumulations of oxides at liquid film surfaces increase surface viscosity, which then slows down drainage [12]. Weigand carried out a quantitative study of the effect of oxide content on stabilisation by varying the oxide content in various aluminium powders [10–13]. In later studies, it was confirmed that the oxide content significantly influences maximum expansion by manipulating the oxide content of Al powders [14]. These results suggest that oxides are surface active and cover the surface of the Al films. If the content is too low, the growing inner surface of the liquid foam cannot be covered completely and surface tension rises locally, triggering rupture events, which then decrease the surface area and prevent the foam

A. Chethan · J. Banhart
Technische Universität Berlin, Hardenbergstr. 36, 10623 Berlin, Germany

A. Chethan · B. S. Murty
Department of Metallurgical and Materials Engineering, Indian Institute of Technology Madras, Chennai 600036, India

F. Garcia-Moreno (✉) · N. Wanderka · J. Banhart
Helmholtz-Zentrum Berlin für Materialien und Energie, Hahn-Meitner-Platz 1, 14109 Berlin, Germany
e-mail: garcia-moreno@helmholtz-berlin.de

from reaching maximum expansion. The role of oxides for stabilising Al foam was further studied by Körner et al. [8]. Powder with low oxide content foamed with lower expansion and a higher degree of drainage. In metallographic analyses of precursor materials and foams, oxides were observed to form an interconnected network. A proposed model assumes that the original oxide network in the pressed powder is fragmented during foaming. Fragments cluster together and form networks of particles, which freely float in the melt. This network of particles is infiltrated by liquid and can bear mechanical forces. The network of particles is completely wetted by the melt and is therefore confined between the two interfaces of each film. The confinement together with the mechanical stability of the network of particles creates a repulsive force, which prevents the films from thinning.

Although most researchers have focused their work on foaming aluminium alloys, the basic principles of foaming technology have been transferred to other low-melting metals such as zinc [15–17], lead [18] and even gold alloys [19]. Zinc foam has shown promising application potential in filling hollow steel sections to improve their stiffness. [20–22]. This is facilitated by the low foaming temperature of Zn, making it suitable for usage of alternative blowing agents [23]. The high expansion and very regular cell structure shown by zinc [24] makes it a promising area for research such as for the investigation of nucleation [25]. The work presented here focuses on the effect of oxide content of zinc powder on the expansion and stability of foam, and of the formation of satellite pores.

Experimental

Materials

Zinc powder supplied by the manufacturer Ecka Granules GmbH, Fürth, had a particle size D_{50} of 30 μm and 99.5 wt% purity. Another powder supplied by Grillo Werke AG, Goslar, exhibited a particle size D_{50} of 120 μm and a purity of 99.995 wt%. This high purity is essential for its use in batteries. TiH_2 supplied by Chemetall GmbH, Frankfurt, with D_{50} of 5 μm and 98.8 wt% purity was used as blowing agent.

Annealing in oxidising and reducing atmosphere was carried out on the Grillo powder to vary its oxide content. Oxidation was performed by annealing powder in air at 300 °C for either 2, 6 or 12 h. Reduction was achieved by annealing the powder in a reducing atmosphere (3% H_2, 97% Ar) at 300 °C for 3 h. The oxygen content of the powders was determined with carrier gas hot extraction (Horiba EMGA 620 WC).

Experimental procedure

Precursors were prepared by mixing zinc powder with 0.6 wt% TiH_2, a content that had been found to be suitable for foaming zinc [26]. This powder blend was compacted uniaxially for 300 s at 350 °C and 300 MPa. The precursors were foamed in an X-ray transparent furnace, which allows in situ observation of expansion as a function of both temperature and time [27]. The precursor was heated to 430 °C and held at this temperature until the sample had fully expanded. After holding, the foam was allowed to cool down to room temperature before collapse sets in. The temperature was recorded once every second throughout the experiments. Foam evolution was visualised by recording X-ray images once every 2 s. The computer analysis software AXIM was used to analyse the acquired images and provided projected areas $A(t)$ of the expanding foam at any given instant. The ratio of the projected area to the initial area, $A(t)/A_0$, can be correlated to volume expansion $V(t)/V_0$ by using the relation $V/V_0 = (A/A_0)^{3/2}$, which, however, is only strictly valid for foams maintaining the same shape of the precursors, but here a good approximation.

The microstructure of the foams was characterised by both optical and scanning electron microscopy (SEM) equipped with an energy dispersive X-ray spectrometer (EDX) for chemical analysis. A Philips CM30 transmission electron microscope (TEM) was used to visualise and characterise the oxides. Samples for TEM were prepared with an Ultramicrotom Cell. 2D pore size distributions and shape analyses of the cells were determined by using the software Image Tool [28]. Pore roundness is defined as $4\pi A/P^2$, where A is the 2D pore area and P the pore perimeter. The maximum value of 1 corresponds to a circle, smaller values to less round objects.

Results

Influence of oxide content on the expansion behaviour

The measured oxide content of the as-received zinc powders was 0.092 wt% for the Ecka powder and 0.039 wt% for powder manufactured by Grillo. The area expansion curves of precursors based on both these powders are shown in Fig. 1. The precursor based on Ecka powder expanded to a higher maximum value of $A/A_0 = 5.2$ than the precursor made from Grillo powder that only reached 3.5. The rate of expansion is also found to be higher for Ecka samples for most of the time. On continued foaming, the Ecka sample collapsed to $A/A_0 = 3.5$ and the Grillo sample to 2.7. With increase in expansion rate, the maximum expansion increased and less pronounced collapse is

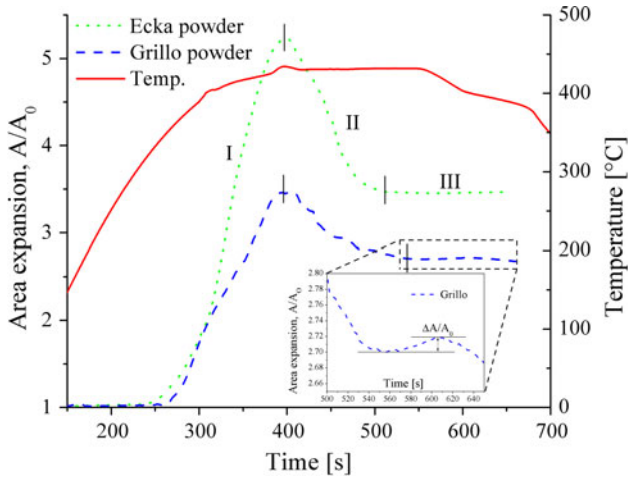

Fig. 1 Expansion curve of precursors made from either Grillo or Ecka powers. *Inset* regime of solidification expansion ($\Delta A/A_0$) marked by an *arrow*

found. This effect can be correlated to the higher oxide content of the Ecka precursor.

The entire foaming process as seen in Fig. 1 can be divided into three stages. The first constitutes the region of foam expansion (I), a continuous expansion region. The second is the foam collapse region (II), in which the foam begins to collapse and about 30–40% reduction in A/A_0 is observed. After this contraction the sample is cooled at constant rate, leading to a third region (III), in which the sample first re-expands slowly (see arrow) before it continues shrinking again. Such solidification expansion was first found for Al and Al alloy foams in the cooling stage of foaming where it can be very high (up to $\Delta A/A_0 = 0.35$) [29], whereas the effect is smaller by the sample here tested ($\Delta A/A_0 = 0.02$–0.08). The reasons for solidification expansion are described in [30].

To explore the effect of oxide content on foaming, the oxide content of Grillo powder was varied by annealing in air or reducing atmosphere. Figure 2a show the oxygen content of annealed powder as a function of annealing time. On oxidising for 12 h, the oxygen content in zinc powder increased from 0.039 to 0.061 wt%, whereas 3 h reduction lowered the oxygen content to 0.026 wt%.

The maximum expansion of precursors made from annealed powder is plotted versus oxygen content in Fig. 2b. It is observed that an increased oxide content from 0.039 to 0.061 wt% leads to a higher maximum expansion of 3.59 to 4.80, respectively. Consequently, the precursor made from the powder with the reduced oxide content expanded less.

Nature of oxides in the Zn foams

Figure 3a and b shows the back-scattered electron image (BSE) of the precursor made from untreated Ecka powder

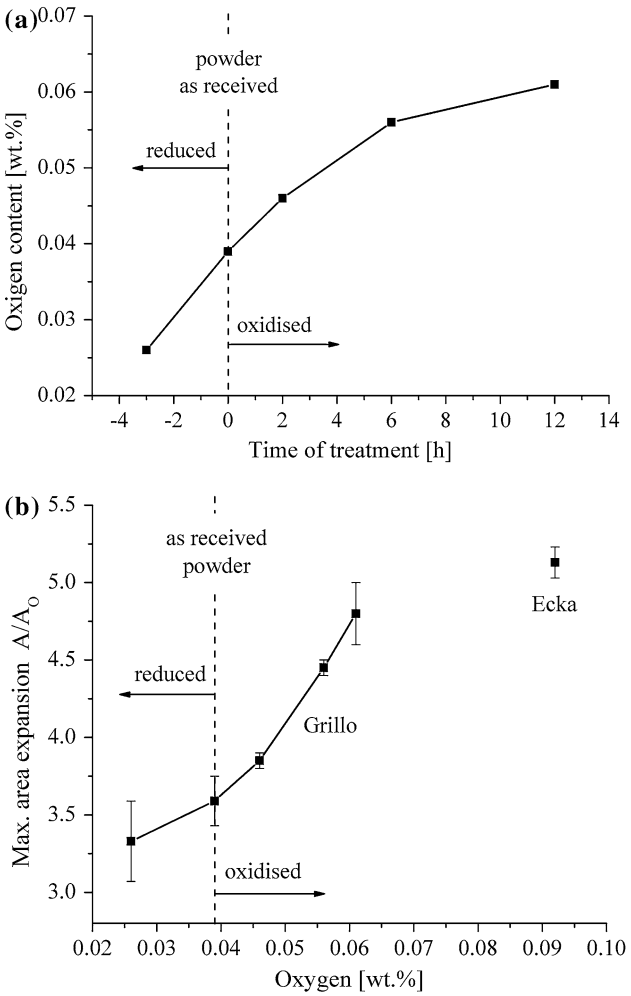

Fig. 2 **a** Variation of the oxide content in Grillo powder by either oxidation or reduction treatment for a given time ($t < 0$ stands for reduction). **b** Effect of oxide content of the precursor on the expansion of foam made from either Grillo or Ecka powers

and the EDX map of the same region. It is observed that oxides are mainly located at the grain-boundaries. Figure 3c is the magnified image of a cell wall containing small embedded pores which we shall call 'satellite pores', and Fig. 3d is the corresponding EDX map of this region. It illustrates that oxides completely cover the inner surface of satellite pores and patches are observed on the main pore walls. Figure 4a shows a BSE image of the inner surface of the foam made from precursor based on as-received Grillo powder. Oxides are seen as small patches, distributed uniformly on the surface of the pore and ranging from 10 to 20 μm in size. In contrast, on the pore surface of the sample made from powder oxidised for 6 h, see Fig. 4b, the oxide clusters are denser and cluster sizes range from 100 to 250 μm.

The oxide distribution across the foam is found to be non-uniform: a metallographic section of the foam is shown in Fig. 5. It is observed that oxide clusters are

denser at the outer surface up to a depth of 2 cm and less dense towards the centre, indicating that the liquid metal has reacted with atmospheric oxygen and has been oxidised during foaming.

TEM images of the foam section made with as-received Grillo powder show two types of oxide morphologies. Figure 6a displays oxides as small hexagonal particles (white) distributed randomly in the metallic matrix with particle sizes ranging from 20 to 200 nm by foams made from untreated powder. In another region, see Fig. 6b, the oxides are seen as clusters (black) with cluster sizes from 0.5 to 2 μm. Selected area diffraction (SAD) revealed that the oxide was ZnO with wurtzite structure.

Micrographs of the foam made from powder oxidised for 6 h show even clearer that oxides are fine hexagonal particles (dark in contrast) distributed randomly in matrix, see Fig. 7, in addition to some acicular-shaped oxides. The SAD pattern analysis (not shown here) of these acicular particles showed that they are ZnO_2 with pyrite structure.

Influence of process parameters on foam structure

Metallographic sections of the foams revealed two types of pores as shown in Fig. 8. The main pores (marked 'A' in Fig. 8) form the major volume of the gas phase and mainly determine the properties of the foam. The average 2D diameter of the main pores varies from 2 to 4 mm, with a maximum of about 6 mm. Satellite pores (labelled 'B' in

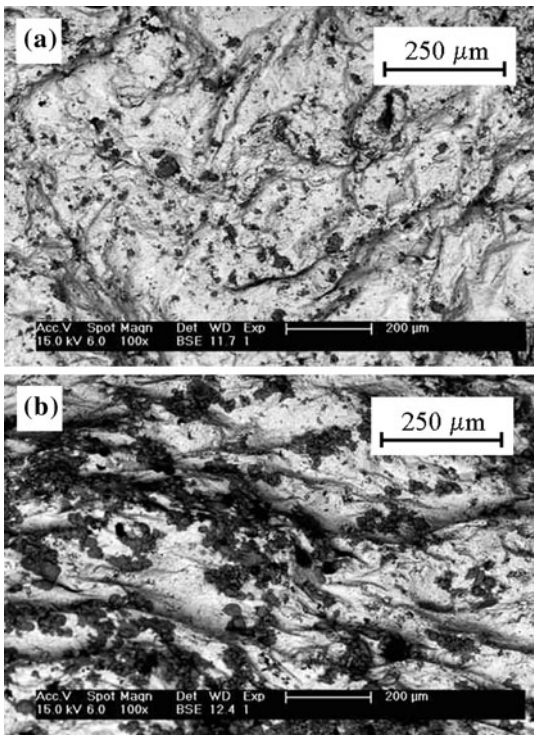

Fig. 4 Back-scattered electron image (BSE) of **a** oxide cluster on the surface of the pore of a foam made from as-received Grillo powders (oxide content: 0.039 wt%) and **b** from powder oxidised for 6 h (oxide content: 0.056 wt%)

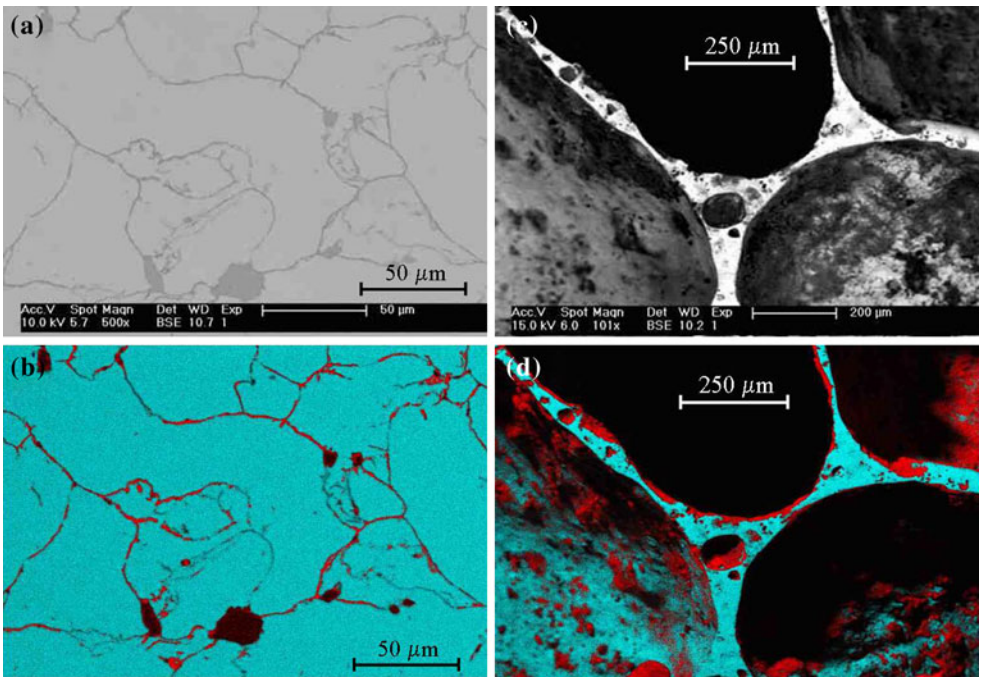

Fig. 3 **a** Back-scattered electron image (BSE) of the made from Ecka powder and **b** the corresponding EDX map of the same region (*cyan/light grey* zinc, *red/dark grey* oxygen-enriched areas). **c** Back-scattered electron image (BSE) of a cell wall cross-section containing satellite pores and **d** the EDX map of the same region (*cyan/light grey* zinc, *red/dark grey* oxygen-enriched areas) (Color figure online)

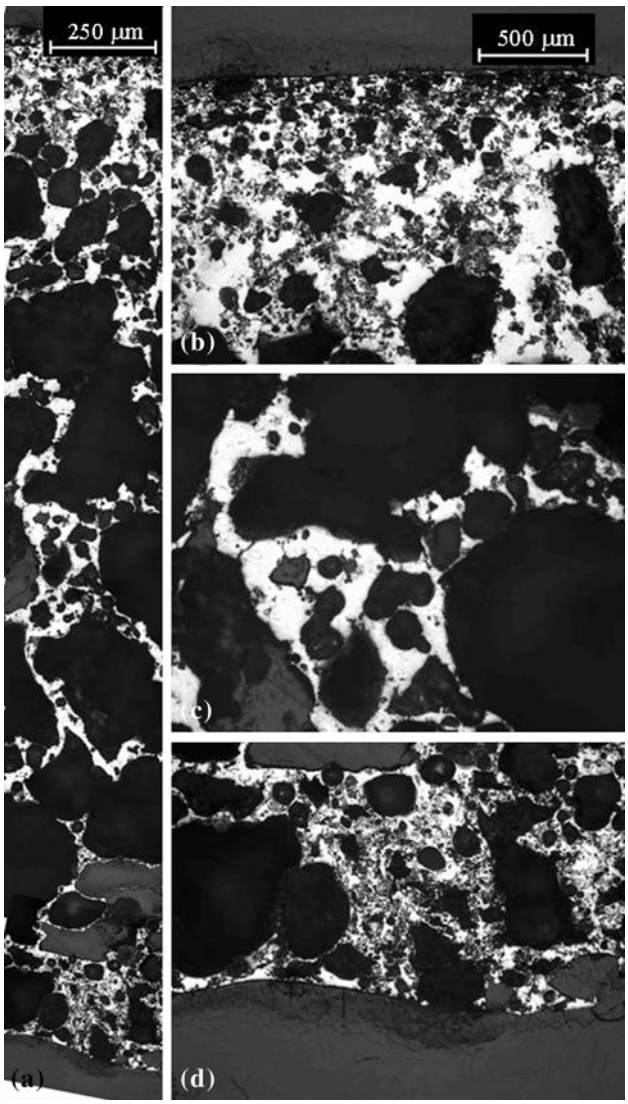

Fig. 5 Back-scattered electron image (BSE) of a foam cross-section (Ecka powder oxide content: 0.092 wt%). **a** overview, **b** top, **c** middle and **d** bottom part magnified

Fig. 8) are smaller when compared to main pores and are located in the cell walls, triple points and Plateau borders. Their size is about 20% of the main pores, i.e. mostly below 1 mm. These pores are very round and smooth compared to the main pores. An analysis of the area of the satellite pores revealed that they cover about 10% of the total solid area of the foam. Pore roundness analysis showed that the main pores are elongated in the direction perpendicular to the pressing direction with an average roundness of ~ 0.8.

To study the formation, growth and stability of satellite pores, the foaming process was interrupted at different stages and metallographic investigations were carried out. Foam collapse was allowed by keeping the foaming temperature over 400 s after reaching the maximal expansion. Figure 9a–d shows SEM images of the pores at different stages of foaming.

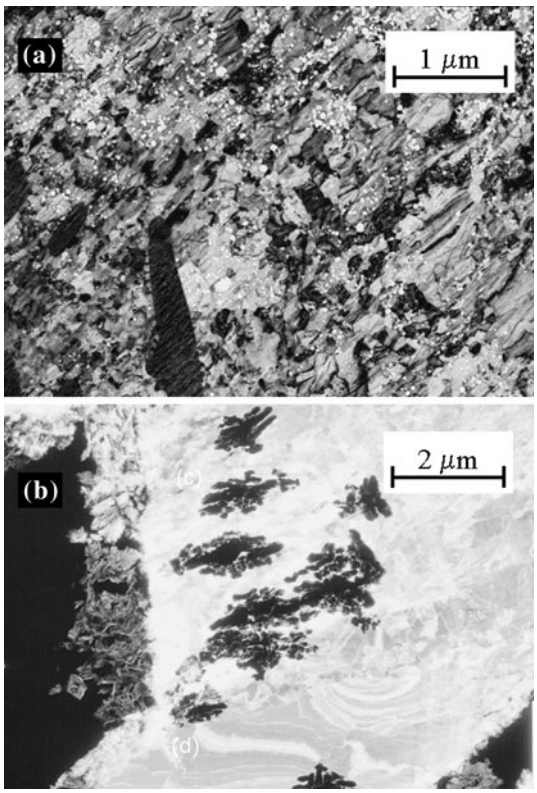

Fig. 6 TEM images showing different oxide morphology in the foam made from as-received Zn powder (Grillo powder, oxide content: 0.039 wt%). **a** Fine hexagonal particles (*bright in contrast*) distributed in bulk of foam. **b** Cluster of oxide (*dark in contrast*)

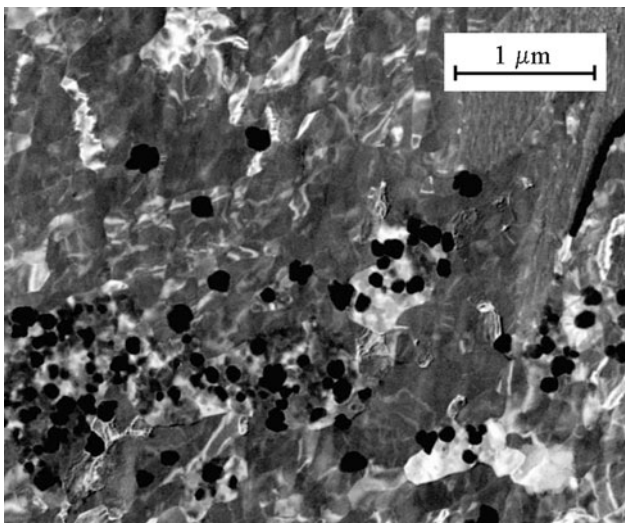

Fig. 7 TEM image showing the oxide particle morphology in a Zn foam made from Grillo powder oxidised for 6 h (oxide content: 0.056 wt%). Fine hexagonal particles (*dark in contrast*) are distributed in the bulk of the foam

Stage I—Initial expansion: it is observed that satellite pores of <50 µm are formed in both cell walls and Plateau borders in this initial stage of foam expansion, see Fig. 9a.

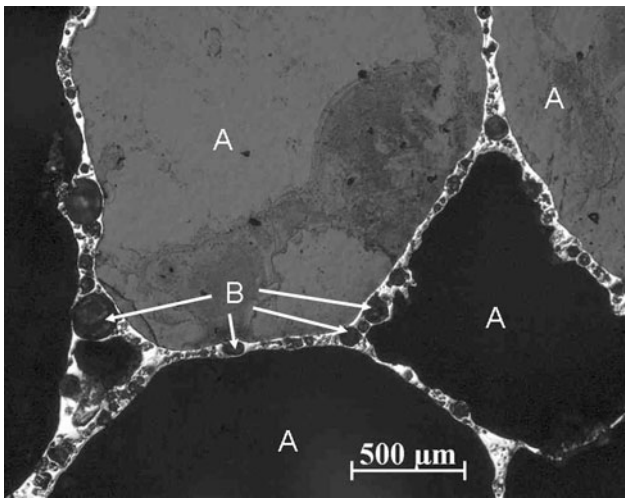

Fig. 8 Metallographic cross-sections of foam made from Ecka powder (oxide content: 0.092 wt%, expansion factor: 910%), *A* main pores, *B* satellite pores

Stage II—Maximum expansion: in this stage, the satellite pores grow to a size of 150–200 µm. Formation of new satellite pores is observed in the walls separating main pores and satellite pore Fig. 9b, i.e. satellites of satellites occur.

Stage III—Initial stage of collapse: the main pores start shrinking and collapsing in this stage, and trigger the collapse of the entire foam. In contrast, satellite pores continuously grow to diameters ranging from 300 to 400 µm. Nucleation of new satellite pores is also observed, see Fig. 9c.

Stage IV—Final stage of collapse: in this stage, the foam has completely collapsed, but the satellite pores are still intact and round in shape, with no change in size as compared to the previous stage, see Fig. 9d.

It was observed that satellite pores are stable and grow throughout the foaming process, in contrast to the main pores that collapse after maximum expansion. To substantiate this observation, the effect of cooling rate on the satellite pores was analysed. For this, foams were cooled by varying the cooling airflow and power of the heater. At the cooling rate of 45 K/min, satellite pores are observed in the cell wall and Plateau borders with a predominant size of $\approx$250 µm, but fine pores are also seen, Fig. 10a. At the cooling rate of 29 K/min, see Fig. 10b, satellite pores grow to an average size of $\approx$400 µm and considerable growth is also observed for the finer pores compared to the higher cooling rate. The main cells already collapse at the cooling rate of 14 K/min while the satellite pores continue to grow to a size of the order of 600 µm, see Fig. 10c. At the lowest cooling rate studied, 5.3 K/min, heavy collapse of the foam cells is observed see Fig. 10d. However, few satellite pores appear that have grown to a size of 700 µm, but many of the satellite pores disappear along with the collapse of cells.

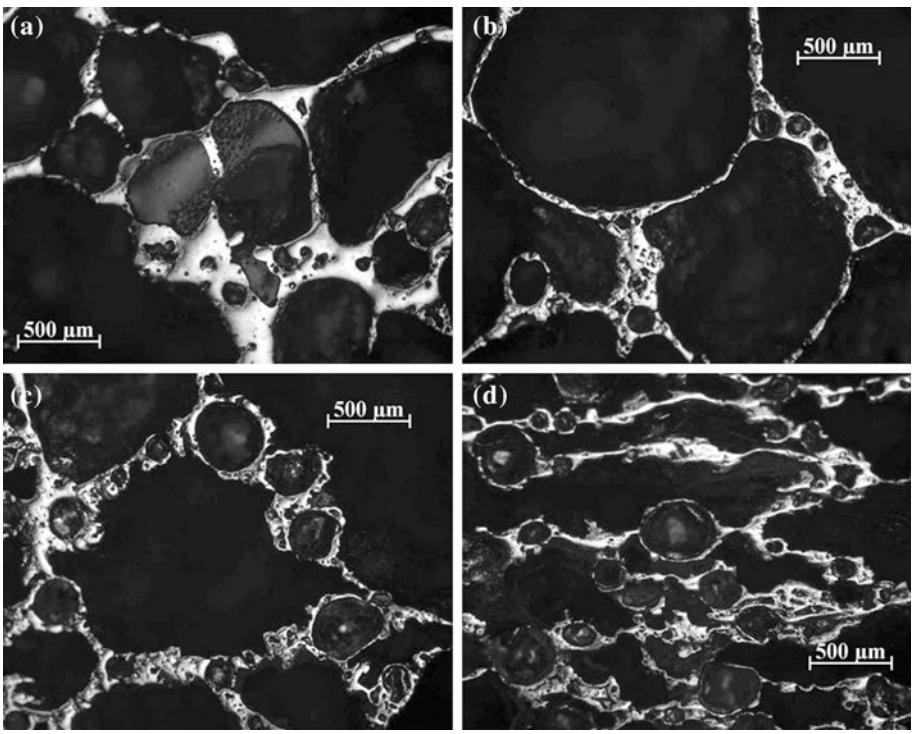

Fig. 9 Metallographic cross-sections of foam made from precursor based on Grillo powder (oxide content: 0.039 wt%) solidified at different stages of foaming. **a** stage I: Initial stage of expansion (395%), **b** stage II: maximum expansion (546%), **c** stage III: initial stage of collapse (349%) and **d** stage IV: advanced stage of collapse (304%)

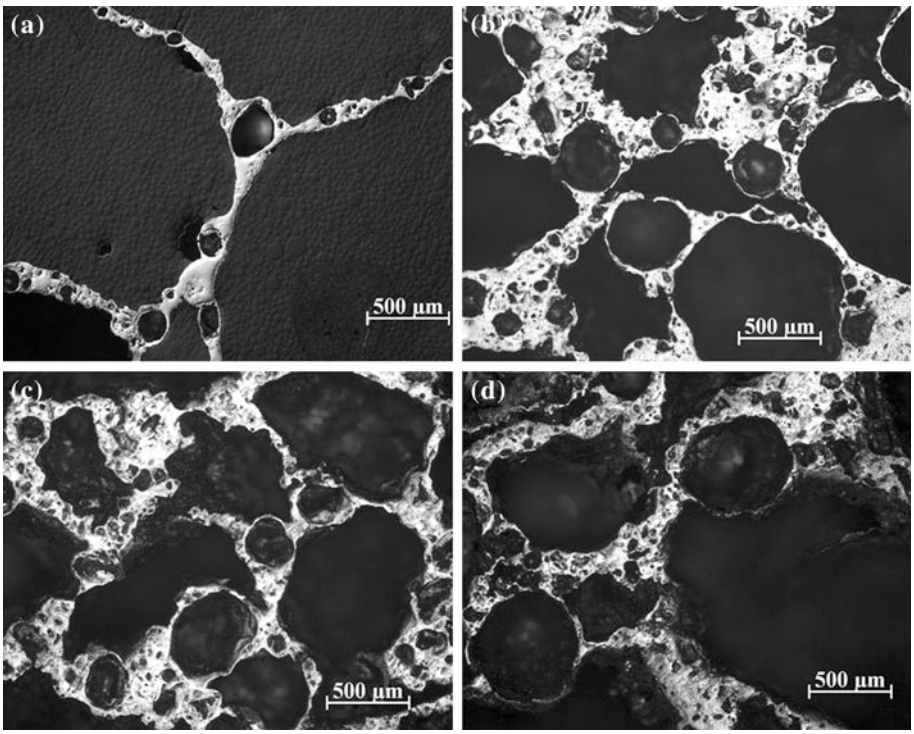

Fig. 10 Metallographic cross-sections of foam made from precursor based on Grillo powder at different cooling rates: Cooling rate of **a** 45 K/min, **b** 29 K/min, **c** 14 K/min and **d** 5.3 K/min

Discussion

Stabilisation by oxides

The experiments carried out clearly reveal that the expansion and stability of zinc foams depends on the oxide content of the starting powder, which can vary depending on the supplier or can be adjusted. As the oxide content of the foam precursor increased after oxidising the powders before compaction (Fig. 2a), both maximum expansion and expansion rate increased (Fig. 2b). The high rates of collapse shown in Fig. 1 may be a result of the high density of zinc.

The oxides present on the surface of the powder may be fractured during hot pressing and form clusters during melting of the powder compact. Apart from this, during foaming liquid metal reacts with the atmosphere and forms further oxides. Oxides are seen as clusters distributed in the cell walls of the foam. TEM images revealed nano-sized oxides (Figs. 6, 7). These clusters of oxide particles could increase the bulk viscosity of liquid metal and hinder drainage of liquid through the foam structure. Networks of oxides as observed in aluminium-based foams [9] are not observed in zinc-based foam, but similar clusters [14]. Major volumes of oxide are observed on top of the surfaces of pores where they appear as clusters, see Fig. 4. Such clusters are uniformly distributed over the entire surface and their density increases with the oxide content of the starting material. These partially wettable oxide clusters could locally alter the surface tension of the films, thereby modifying their radius in analogy to the action of particles on a film surface [10]. It has been recently established that a contact angle of about 60–90° is better for particles to stabilise the foam. At this partially wettable state, the stabilising particles remain at the interface between the gas and liquid rather than either completely in the liquid (complete wettability, contact angle close to 0°) or in the gas (complete non-wettability, contact angle close to 180°). Such a situation is known to stabilise the foam [10]. Clusters of oxides increase the viscosity of liquid Zn and reduce the capillary driven flow, hence delaying the rupture of films.

Satellite pores

It is observed that satellite pores are almost round and stable throughout foaming when compared to the main pores, which often collapse after maximum expansion has been reached, see Figs. 8, 9 and 10. This high stability of satellite pores can be attributed to oxides completely covering their surface as seen in Fig. 3d. The very low diffusivity and solubility of hydrogen in zinc may lead to entrapment of hydrogen in the cell walls and prevent the gas from diffusing to the main pores, thus leading to the formation of satellite pores. The diffusion coefficient of hydrogen in pure zinc close to the melting point is of the order of 10^{-11} cm^2/s [31], with a solubility of about 6×10^{-5} at.% [32]. The diffusion coefficient of hydrogen

in liquid pure Al at 660 °C is 3.2×10^{-3} cm^2/s [33]. The solubility is about 1.2×10^{-3} at.% at the same conditions [34]. The higher diffusivity and solubility of hydrogen in Al and its alloys allows the gas to diffuse quickly from satellite pores to main pores, thus reducing their number in Al foams. Furthermore, satellite pores are supposed to behave as additional stabilisation particles of the foam, as they are covered by oxides.

Pore nucleation takes place at lower temperatures, before the sample starts expanding. Pore formation without locally present blowing agent particles at triple grain junctions has been observed in zinc foam [25]. At that early time the main gas source is not the blowing agent but other gases such as hydroxides or water in form of adsorbates on the surface of the metal powder particles [35]. Adsorbates decompose into hydrogen and oxygen and give rise to pore nucleation and promote the oxidation of the inner part of the pores as observed in a later stage as shown in Fig. 3. At elevated temperatures closer to the melting point, the nucleated pores start growing. Some of the nucleated pores are able to break the inner oxide layer and continue growing driven by the strong gas supply from the blowing agent particles, eventually forming the main pores. However, most of the pores remain well stabilised due to the inner oxide layers that preserve their original round shape and are just displaced to the cell walls, Plateau borders and triple junctions by the pressure exerted by the main pores. This interpretation is supported by the low diffusivity and solubility of hydrogen in molten Zn which hinders hydrogen to diffuse to the main pores. Thereafter, the blowing agent particles (TiH_2) do not act as main gas source for pore nucleation and satellite pores, but for the main pores only. This leads to the conclusion that we obtain two different pore populations, namely satellite and main pores that have a different history.

To prove the above hypothesis, an experiment has been carried out in which Zn powder compact has been heated without a foaming agent under similar foaming conditions that were used with the blowing agent. Interestingly, the sample foamed and the optical micrograph of the resultant foam is shown in Fig. 11. It is very clear from this that it is possible to prepare a Zn foam without a blowing agent, although with only a low porosity. All the pores that are observed in the above image are satellite pores that nucleate and grow.

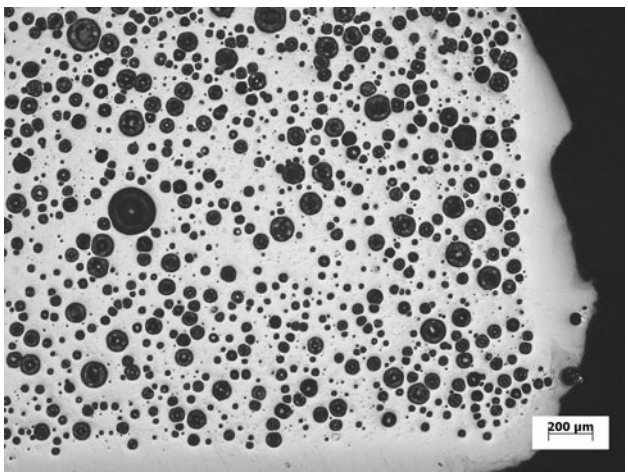

Fig. 11 Optical micrograph of Zn foam obtained without the addition of a blowing agent

Conclusions

1. Zinc foams are stabilised by zinc oxide.
2. There is a clear positive correlation between oxide content and maximum area expansion of Zn foams.
3. Zinc foams exhibit a much larger number of satellite pores than aluminium foams. Their different morphology (small, round and with a completely oxidised surface) and stability against collapse allow for the conclusion that their history is different to that of the main pores and that they behave as a stabilising particle.

Acknowledgements This work was carried out under cooperation of Technical University Berlin and Indian Institute of Technology Madras within the sandwich program of the Deutscher Akademischer Austauschdienst (DAAD). The authors express thanks to Mr. Schubert-Bischoff, Helmholtz-Zentrum Berlin and Dr. Oliver Görke, Department of Ceramics, Technische Universität Berlin for their help in experimentation.

References

1. Ashby MF, Evans AG, Fleck NA, Gibson LJ, Hutchinson JW, Wadley HNG (2000) Metal foams—A design guide. Butterworth-Heinemann, London
2. Banhart J (2001) Prog Mater Sci 46:559
3. Degischer H-P, Kriszt B (2002) Handbook of cellular metals. Wiley-VCH, Weinheim
4. Banhart J (2000) J Metals 12:22
5. Ip SW, Wang Y, Toguri JM (1999) Can Metall Q 38:81
6. Leitlmeier D, Degischer H-P, Flankl HJ (2002) Adv Eng Mater 4:735
7. Haibel A, Rack A, Banhart J (2006) Appl Phys Lett 89:154102
8. Körner C, Arnold M, Singer RF (2005) Mater Sci Eng A 396:28
9. Dudka A, Garcia-Moreno F, Wanderka N, Banhart J (2008) Acta Mater 56:3990
10. Banhart J (2006) Adv Eng Mater 8:781
11. Asavavisithchai S, Kennedy AR (2006) J Colloid Interface Sci 297:715
12. Weber M (1995) Thesis, University of Clausthal, Germany
13. Weigand P (1999) Thesis, University of Aachen, Germany
14. Asavavisithchai S, Kennedy AR (2006) Adv Eng Mater 6:568

15. Banhart J, Weber M, Baumeister J (1995) In: Proceedings of the European conference on advanced PM materials. European Powder Metallurgy Association, Birmingham, pp 201–208
16. Thornton PH, Magee CL (1975) Met Trans A 6A:1801
17. Dasler M, Törnqvist S (2000) Diploma work, Stockholm, Sweden
18. Irretier A, Banhart J (2005) Acta Mater 53:4903
19. Banhart J (2008) Gold Bull 41:251
20. Kovacik J, Simancik F (2001) In: Banhart J, Fleck NA, Mortensen A (eds) Metal foams and porous metal structures. MIT-Verlag, Bremen, pp 355–358
21. Kovacik J, Simancik F (2004) Met Mater 42:79
22. Stöbener K, Weigend M, Rausch G (2003) In: Banhart J, Fleck NA, Mortensen A (eds) Cellular metals: manufacture, properties, applications. MIT-Verlag, Berlin, pp 161–164
23. Mukherjee M, Garcia-Moreno F, Jimenez C, Banhart J (2010) Adv Eng Mater 12:472
24. Banhart J (1999) Europhys News 30:17
25. Banhart J, Bellmann D, Clemens H (2001) Acta Mater 49:3409
26. Rosumek MR (2006) Diploma thesis, Tecnical University Berlin, Germany
27. Garcia-Moreno F, Fromme M, Banhart J (2004) Adv Eng Mater 6:416
28. Software 'Image tool': http://ddsdx.uthscsa.edu/dig/. Accessed 9 Jan 2011
29. Mukherjee M, Garcia-Moreno F, Banhart J (2007) Trans Ind Inst Metals 60:133
30. Mukherjee M, Garcia-Moreno F, Banhart J (2010) Acta Mater 58:6358
31. Cao JL, Li LT, Wu JX, Lu YP, Gui ZL (2002) Corrosion 58:698
32. Okamoto H (1990) In: Massalski TB (ed) ASM, binary phase diagrams, 2nd edn. ASM International, Materials Park
33. Eichenauer W, Markopoulos J (1974) Z. Metallkunde 65:649
34. San-Martin A, Manchester FD (1992) J Phase Equilib 13:17
35. Garcia-Moreno F, Banhart J (2007) Coll Surf A309:264